PAPER

Benchmark experiments of the power law parametrization of the effective ion collecting area of a planar Langmuir probe in low temperature plasmas

To cite this article: Yegeon Lim et al 2022 Plasma Sources Sci. Technol. 31 024001

View the article online for updates and enhancements.

You may also like

- Revolutionizing Our Understanding of AGN Feedback and its Importance to Galaxy Evolution in the Era of the Next Generation Very Large Array K. Nyland, J. J. Harwood, D. Mukherjee et al
- Analysis of the operating parameters of a vortex electrostatic precipitator
 Congxiang Lu (), Chengwu Yi (), Rongjie Yi () et al.
- <u>Seeing-limited Imaging Sky</u> <u>Surveys—Small versus Large Telescopes</u> E. O. Ofek and S. Ben-Ami



Benchmark experiments of the power law parametrization of the effective ion collecting area of a planar Langmuir probe in low temperature plasmas

Yegeon Lim¹, Greg Severn², Chi-Shung Yip³ and Y-c Ghim^{1,*}

- Department of Nuclear and Quantum Engineering, Korea Advanced Institute of Science and Technology, Daejeon 34141, Republic of Korea
- ² Department of Physics and Biophysics, University of San Diego, San Diego, CA 92110, United States of America
- ³ Institute of Plasma Physics, Hefei Institutes of Physical Science, Chinese Academy of Sciences, Hefei 230031, People's Republic of China

E-mail: limpanc@kaist.ac.kr and yeghim@kaist.ac.kr

Received 1 November 2021, revised 23 December 2021 Accepted for publication 19 January 2022 Published 17 February 2022



Abstract

For unmagnetized low temperature Ar plasmas with plasma density ranging from 3×10^8 to $10^{10} \, \mathrm{cm}^{-3}$ and an electron temperature of $\sim 1 \, \mathrm{eV}$, the expansion of the ion collecting area of a double-sided planar Langmuir probe with respect to probe bias is experimentally investigated, through a systematic scan of plasma parameters. In accordance with many existing numerical studies, the ion collecting area is found to follow a power law for a sufficiently negative probe bias. Within our experimental conditions, the power law coefficient and exponent have been parameterized as a function of the normalized probe radius and compared with numerical results where qualitatively comparable features are identified. However, numerical results underestimate the power law coefficient while the exponent is overestimated. Our experimental measurements also confirm that ion-neutral collisions play a role in determining the expanded ion collecting area, thus changing values of the power law coefficient and exponent. This work suggests that a power law fit to the ion collecting area must be performed solely based on experimentally obtained data rather than using empirical formulae from simulation results since material and cleanness of the probe, type of working gas, and neutral pressure may also affect the expansion of the ion collecting area, factors which are difficult to model in a numerical simulation. A proper scheme of analyzing an I-V characteristic of a Langmuir probe based on a power law fit is also presented.

Keywords: planar Langmuir probe, ion sheaths, ion collecting area, power law dependence (Some figures may appear in colour only in the online journal)

1. Introduction

Since its advent about a century ago [1] a Langmuir probe, due to its simplicity, has been one of the most fundamental and

* Author to whom any correspondence should be addressed.

widely used diagnostics [2] to obtain basic parameters such as density, floating and plasma potentials, and electron temperature in low temperature vacuum plasmas. These parameters are inferred based on a current–voltage (I-V) characteristic, where the current is a sum of electron and ion currents collected by an electrically biased Langmuir probe.

Charged particles incident upon the biased conducting probe surface traverse a non-neutral sheath. When an ion-rich sheath is formed by a probe biased negatively with respect to the plasma potential, we assume that the ion flow velocity at the sheath edge is the Bohm velocity, as determined by the well known Bohm criterion [3, 4]. Thus, if we know the collecting area of the probe for incoming ion particles, then the ion flux can be calculated from the measured current, and the plasma density can be inferred if we can calculate the Bohm velocity. The sheath typically expands as the probe bias is swept negatively, such that the effective ion collecting area becomes increasingly larger than the physical probe area. Thickness of the sheath can be crudely approximated by the Child-Langmuir law [5–8]; however, precise determination of it can be extremely difficult depending on a geometry of the surface. This fact, to some extent, undermines the reliability of a Langmuir probe due to uncertainty in the ion collecting area.

Analytic solutions compensating the effect of such an expanded ion collecting area are available only for some limited cases such as probes having a spherical or cylindrical geometry with $r/\lambda_{\rm D}\gg 1$ or $r/\lambda_{\rm D}\ll 1$ [9–14], where r is the relevant probe dimension and the electron Debye length $\lambda_{\rm D}$. For a Langmuir probe with a planar disk tip the situation is more complicated than the cases of cylindrical or spherical probe tips because of an extra dimension and edge effects [15–17]. There are no analytic solutions except for a large probe limit $(r/\lambda_{\rm D}\gg 1)$, which corresponds to one-dimensional planar theory [18]. For a small probe limit $(r/\lambda_{\rm D}\ll 1)$, we can only anticipate that a spherical sheath is formed [19–21] around a planar disk tip.

Lack of such analytic solutions for realistic probe dimensions has motivated many researchers to consider numerical solutions, and the expanded ion collecting area was found to have a power law dependence on the probe bias. For cylindrical and spherical probes, numerically calculated ion current based on Laframboise's work [12] is found to have a power law dependence on the probe bias [22-25]. The power law parameters, i.e. a power law coefficient and a power law exponent, obtained by a fit to a power law to the calculated ion current are presented as a function of r/λ_D [22, 24, 25]. Similar conclusions have been drawn for a planar probe based on particle-in-cell simulations carried by Sheridan [20, 21], where the author has also provided empirical formulae for estimating the expanded ion collecting area. Application of Sheridan's formulae for estimates of ion density have been compared with experimental results [26-28] and other simulations [29]. The main contribution of this work, however, is to benchmark Sheridan's power law model for the additional ion collecting area (owing to the expansion of the sheath) experimentally, comparing power law dependences of the model with experimental measurements for a wide range of basic plasma parameters that systematically vary r/λ_D . To the best of our knowledge, this is the first experimental work to benchmark these critical power law parameters, and further, the first to show experimentally that a power law other than the conventional linear approximation works best.

We find that in the range of bias voltages sufficiently negative to neglect the electron current, a power law dependence for the additional ion collecting area is found as expected from the model, however, surprisingly, the experimentally measured fitting parameters differ from model values, with the discrepancy exceeding the experimental uncertainty. Expressed as a function of r/λ_D , the model power law exponent overestimates the measured value, and model power law coefficient underestimates the measured value.

In this work, we present results verifying that the normalized edge effect area, $\alpha_{\rm EE} \equiv (A_{\rm eff} - A_{\rm phy})/A_{\rm phy}$, i.e. normalized additional area from the physical probe surface area, of a double-sided planar probe indeed follows a power law dependence for sufficiently large negative bias, where A_{eff} and A_{phy} are effective (expanded) ion collecting area and physical probe surface area, respectively. The planar probe used in this work is a thin circular disk, with probe radius $r_{\rm phy}=5$ mm, thickness $h_{\rm phy}\approx 0.07$ mm; and we calculate $A_{\rm phy} = 2\pi r_{\rm phy}^2$, neglecting the edge dimension, the thickness of the probe, as does Sheridan in his models. We justify this approach by its negligible effect on the size of the area, seeing that the correction is approximately 1.4×10^{-2} , i.e. from $(A_{\rm phy} + 2\pi r_{\rm phy} h_{\rm phy})/A_{\rm phy}$. Following Sheridan [20, 21], we think of $\alpha_{\rm EE}$ as the 'edge' effect because the portion of the physical area of the probe, that was justifiable to neglect, grows to such a large fraction of the expanded sheath area that it cannot be neglected, indeed, it becomes the dominant fraction of the whole surface area.

We also present experimentally obtained power law parameters which are compared with Sheridan's formulae for a wide range of normalized probe radius, $\rho \equiv r_{\rm phy}/\lambda_{\rm D}$, and examine asymptotic behaviour of them. As has been shown previously in simulations [30], ion–neutral collisions can also change $\alpha_{\rm EE}$; thus we have also quantitatively investigated how finite collisionality in the presheath and sheath affect $\alpha_{\rm EE}$. For the sake of readers, we also describe the detailed steps we follow to analyse an I-V characteristic measured by a Langmuir probe, which we find consistent with a power law dependence, without utilizing any of empirical formulae suggested by the simulations.

To make our assumptions most transparent, we note that there is a modelling choice to make in order to fit empirical data, which in our case is the asymptotic form of the ion branch of the *I–V* characteristic measured by a Langmuir probe for large negative bias voltage. Empirically we find, free and clear of previous theoretical efforts (including simulation work under this term) that our data is well fit by a simple monomial dependence on the bias voltage normalized to the electron temperature. Other modelling choices obviously are possible, except that this choice affords the best comparison with Sheridan's work. And so, while we do invoke Sheridan's form [20] of the monomial, we find and present in this work the *experimental* result that a simple power law fit is a good one, and the *empirical parameters* that characterize that fit, which we compare with the simulations discussed above.

Theoretical background is presented in section 2 followed by the experimental setup for this work in section 3. Section 4

describes detailed steps on how to analyse the I-V characteristics from which a power law dependence is found to arise, and which is compared with the conventional linear approximation and Sheridan's empirical formulae. In section 5, we present the key findings of this work which are (1) a thorough experimental verification of a power law dependence for a wide range of plasma parameters and (2) a parameterization of the power law parameters as functions of $r_{\rm phy}/\lambda_{\rm D}$, where the goodness of the fits are quantified by a mean squared error analysis. Further, we discuss ion–neutral collision effects on the expanded ion collecting area in section 6. Our conclusion and summary are presented in section 7.

2. Theoretical background

A typical current–voltage (I-V) characteristic obtained by a Langmuir probe in plasmas can be divided into three regions. If the probe bias $\phi_{\rm b}$ is more positive than the plasma potential $\phi_{\rm p}$ ($\phi_{\rm b}>\phi_{\rm p}$), then the probe current is dominated by electrons. On the other hand, for a case of $\phi_{\rm b}\ll\phi_{\rm p}$ the probe collects only positively charged ions. In the intermediate region where $\phi_{\rm b}$ is slightly smaller than $\phi_{\rm p}$, the probe current consists of both electron and ion contributions. In this work, we are primarily interested in the regions where the ions are collected to experimentally investigate behaviour of an expanding ion collecting area for a double-sided planar Langmuir probe.

Far from boundaries, the ion saturation current I_i^{sat} in a collisionless plasma with a singly charged and cold ion species is expressed as [31]

$$I_{\rm i}^{\rm sat} = e\kappa n_0 A_{\rm phv} C_{\rm S},\tag{1}$$

where n_0 is plasma density in the bulk plasma, $C_{\rm S} = \sqrt{T_{\rm eff}/m_{\rm i}}$ is the Bohm speed with, in our case, an effective electron temperature $T_{\rm eff}$ (see section 4.1), $m_{\rm i}$ is the ion mass, and e, the electron charge. The constant $\kappa \approx 0.6$ arises from the potential drop, $\Delta\phi$, between the bulk plasma potential and the sheath edge potential of the sheath surrounding the probe tip, where according to the Bohm criterion, $e\Delta\phi \geqslant T_{\rm eff}/2$. Following Chen [32], assuming thermal equilibrium for the electron population, the electron density falls by this factor relative to the bulk electron plasma density as $n_{\rm e}/n_0 \approx \exp(-e\Delta\phi/T_{\rm eff})$. And the ion and electron densities are expected to be the same up to the sheath edge. This density drop becomes $\exp(-1/2) \approx 0.6$.

The motivation for this expression of the ion saturation current is that a non-neutral, ion-rich sheath region is thought to envelop the probe surface. It is thought that the space charge effect is least at the bulk plasma potential, and thus the conventional method [26, 33, 34] for obtaining the ion density from the I-V characteristic has been simply to extrapolate linearly from an arbitrary ion current (for sufficiently negative bias) to its value at ϕ_p , thus 'measuring' the ion saturation current of equation (1), from which the ion density may be estimated. This method, however, does not reliably agree with the

measurement of the electron density [2, 26]. Sheridan's reasoning provides a correction to this approach. He noted [20] that $\kappa \approx 0.6$ applies strictly only for a spherical sheath, and that sheath expansion needs to be carefully modelled through simulations [20, 21] for the given geometry of the actual probe surface, resulting in an effective ion current collecting area as a function of the negative probe bias potential.

In this work, as defined earlier, the *effective* collecting area is denoted as $A_{\rm eff} = (1 + \alpha_{\rm EE})A_{\rm phy}$ where $\alpha_{\rm EE}$ encapsulates the expanded area of the sheath edge [21]. Thus, the actual collected ion current is

$$I_{\rm i} = (1 + \alpha_{\rm EE})I_{\rm i}^{\rm sat}. \tag{2}$$

Sheridan's numerical simulations found that a double-sided planar probe (thin circular disk) has a power law dependence of the normalized edge effect area on the bias voltage as follows [20, 21]:

$$\alpha_{\rm EE} = a\eta^b,$$
 (3)

where $\eta=-e(\phi_{\rm b}-\phi_{\rm p})/T_{\rm eff}$ is the normalized bias voltage. Sheridan found that the power law coefficient a and exponent b can be empirically formulated by fitting a power law to numerical results as functions of the normalized probe radius $\rho=r_{\rm phy}/\lambda_{\rm D}$, as defined earlier. Here, $\lambda_{\rm D}=\sqrt{\varepsilon_0T_{\rm eff}/e^2n_0}$ is the Debye length with the vacuum permittivity ε_0 . For the sake of readers, we write down the formulae here, which are

$$a(\rho) = 2.28\rho^{-0.749},$$

 $b(\rho) = 0.806\rho^{-0.0692},$ (4)

for $10 \leqslant \rho \leqslant 45$ [20], and

$$a(\rho) = \frac{6.425}{\rho} \left(1 - \frac{6.835}{\rho} \right),$$

$$b(\rho) = 0.5928 \left(1 + \frac{2.703}{\rho} \right),$$
(5)

for $25 \le \rho \le 200$ [21], where specific numbers are determined by the simulation results given empirical forms of equations.

Following Sheridan's work [20, 21], we experimentally show how well $\alpha_{\rm EE}$ depends on a power law and discuss how to determine the power law coefficient a and exponent b solely based on experimental data, i.e. without relying on equations (4) or (5). Thus, our approach will not produce bias errors due to incompleteness, if there are any, of the Sheridan's formulae.

3. Experimental setup

We have conducted experiments in the low temperature cylindrical plasma device MAXIMUS (magnetic X-point simulator system) [35] in absence of axial current carrying rods. As a result, there are no poloidal magnetic fields except the multidipole configuration. The cylindrical multidipole

⁴ Possible variation in the value of κ [29] can be absorbed into the normalized edge effect area $\alpha_{\rm EE}$ in equation (2) for $\alpha_{\rm EE}\gg 1$.

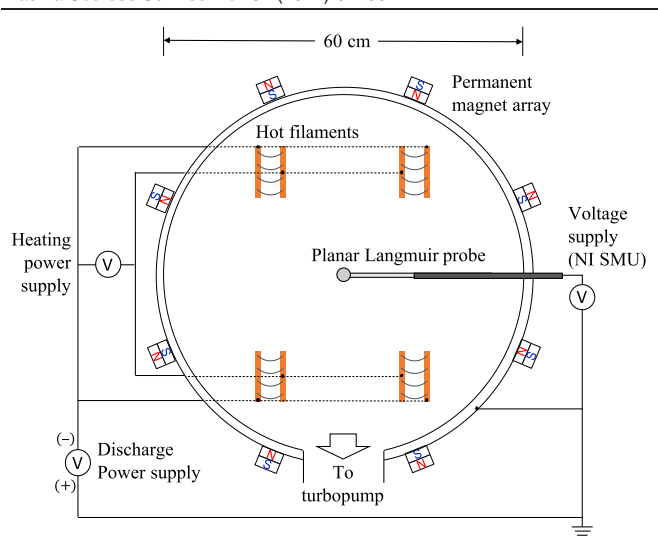


Figure 1. A schematic diagram of the multidipole chamber with DC plasma sources (hot filaments) and a double-sided planar Langmuir probe. I-V characteristics of the Langmuir probe are obtained by a National Instruments (NI) PXIe-4137 source measure unit (SMU).

chamber is filled with 0.13 Pa (≈ 1.0 mTorr) of Ar gas for most results presented in this work⁵ where a typical base pressure in the chamber is 5×10^{-4} Pa ($\approx 4 \times 10^{-3}$ mTorr).

DC plasmas in the cylindrical chamber are generated by energetic primary electrons emitted from negatively biased hot thoriated tungsten filaments installed on the chamber wall as shown in figure 1. Bias voltage on the filaments was fixed at -60 V. Emitting electron current is varied from 0.002 to 2.2 A, which is controlled by a filament heating power, to cover a wide range of the normalized probe radius ρ . These conditions generate plasmas with the density of 10^8-10^{10} cm⁻³, bi-Maxwellian (two-temperature) electrons with $T_{\rm eff} \sim 1$ eV and cold ions.

A tantalum double-sided planar Langmuir probe with a radius given earlier as 5 mm was located at the radial centre of the cylindrical chamber and axially ~ 50 cm away from the hot filaments. The probe surface faced the side (cylindrical) wall⁶ to minimize direct incidence of the energetic primary electrons to the surface. The probe tip was thermally heated by applying positive bias voltage with respect to the plasma potential for every tens of voltage sweeps to maintain the probe surface clean. This corresponds to a few minutes between the sequence of the probe cleaning which is much shorter than the typical characteristic time for surface contamination (roughly hours). We swept the bias voltage $\phi_{\rm b}$ on the Langmuir probe from -150 to 10 V, obtaining ten I-Vcharacteristics for an ensemble average. Figure 2 shows an example of an ensemble-averaged I-V characteristic for this study.

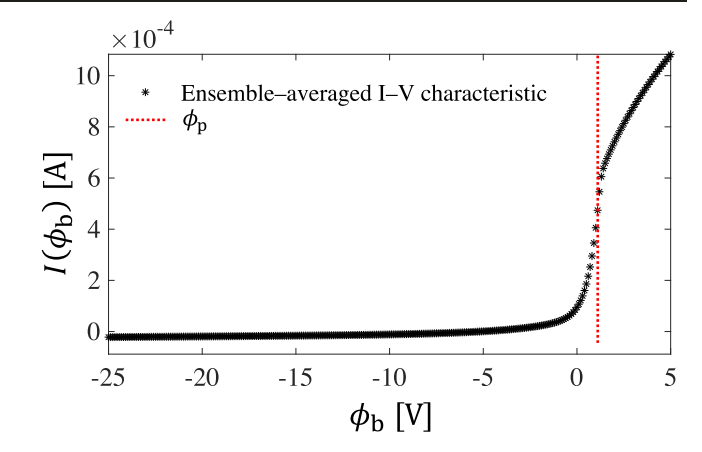


Figure 2. An example of an ensemble-averaged I-V characteristic measured by the Langmuir probe (black asterisks) and an estimated plasma potential ϕ_p (red vertical dotted line).

4. Analysis of double-sided planar Langmuir probe, including a novel method of analyzing *I–V* characteristics

Before we discuss how well the experimentally observed normalized edge effect area followed a power law dependence as in equation (3), we explain in detail our method of analyzing I-V characteristics [35] and compare it with other existing methods.

4.1. Novel iterative method to find plasma parameters using the I–V characteristic

Accurate electron information can be obtained from an I-V characteristic only if one can remove ion current contribution properly which, in turn, depends on electron information, for instance the Bohm speed $C_{\rm S}$. This inevitably introduces a requirement of iterative approach for analyzing I-V characteristics.

First, from a measured ensemble-averaged I-V characteristic the plasma potential $\phi_{\rm p}$ is determined using an inflection point method, and we let the initial electron saturation current $I_{\rm e}^{\rm sat}$ to be a measured current at $\phi_{\rm b}=\phi_{\rm p}$. The initial electron temperature is set to be an inverse slope of a linear fit to a partial domain $(\phi_{\rm p}-1<\phi_{\rm b}\,[{\rm V}]<\phi_{\rm p})$ of a semi-log plot of the I-V characteristic. During this first iteration, the initial electron temperature is treated as the effective electron temperature $T_{\rm eff}$ to estimate initial values of the Bohm speed $C_{\rm S}$ and the plasma density n_0 from $I_{\rm e}^{\rm sat}$, and to calculate the normalized $\phi_{\rm b}$, i.e. $\eta=-e(\phi_{\rm b}-\phi_{\rm p})/T_{\rm eff}$.

An ion current $I_i(\eta)$ is estimated by the best fit to the I-V characteristic using equations (2) and (3) with the values of the estimated n_0 and $T_{\rm eff}$. Notice that using n_0 from $I_{\rm e}^{\rm sat}$ for a fit to I_i means that we implicitly constrain the quasi-neutrality of plasmas. We let the power law coefficient $a(\rho)$ and exponent $b(\rho)$ be free parameters for the fit, rather than using equations (4) or (5). Determining a valid fitting range is discussed in section 5 together with comparisons of the determined free parameters against the Sheridan's empirical models. Once we have a

⁵ We have only varied neutral pressures for figures 9 and 10 in section 6 to examine how collisions affect the ion collecting area.

 $^{^6}$ Inconsistent probe angle drawn in figure 1 with the text is for clear visualization.

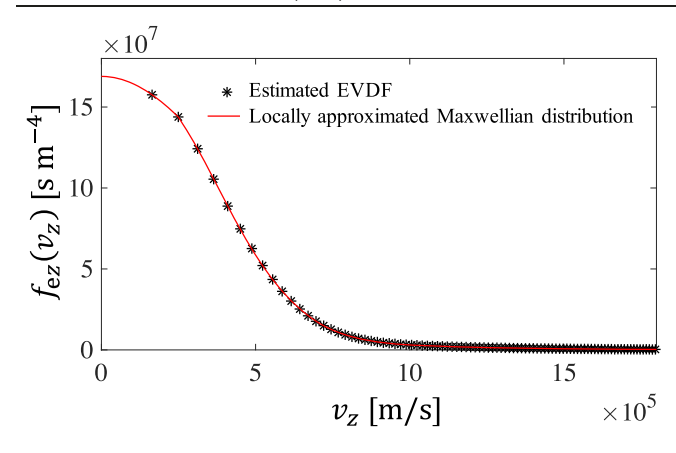


Figure 3. An example of an estimated EVDF using equation (7) (black asterisks) with a locally approximated Maxwellian distribution (red line) using the data shown in figure 2.

fitted $I_i(\eta)$, we subtract it from the I-V characteristic to obtain an electron current $I_e(\eta)$.

An electron velocity distribution function (EVDF) $f_e(\vec{v})$ can be obtained from the electron current I_e using a following relation when $\phi_b < \phi_p$ [18]:

$$I_{e} = eA_{phy} \int_{-\infty}^{\infty} \int_{-\infty}^{\infty} dv_{x} dv_{y} \int_{v_{min}}^{\infty} dv_{z} v_{z} f_{e}(\vec{v})$$

$$= eA_{phy} \int_{v_{min}}^{\infty} dv_{z} v_{z} f_{ez}(v_{z}), \qquad (6)$$

where we let the surface of an *one-sided* planar probe face plasmas in $-\hat{z}$ direction and have assumed that the EVDF in bulk plasmas is isotropic and separable with $f_{\rm ez}(v_z) \equiv \int_{-\infty}^{\infty} \int_{-\infty}^{\infty} {\rm d}v_x \, {\rm d}v_y f_{\rm e}(\vec{v})$ and $\frac{1}{2} m_{\rm e} v_{\rm min}^2 = -e(\phi_{\rm b} - \phi_{\rm p})$. $m_{\rm e}$ is the electron mass. Therefore, we can estimate $f_{\rm ez}(v_z)$ for $v_z > 0$ from the obtained $I_{\rm e}$ as [36]

$$f_{ez}(v_z) = \frac{m_e}{A_{\text{phy}}e^2} \frac{dI_e}{d\phi_b} \bigg|_{\frac{1}{2}m_e v_z^2 = -e(\phi_b - \phi_p)}.$$
 (7)

An example of an estimated EVDF is shown in figure 3. Note that equation (7) is also valid for $v_z < 0$ for an isotropic distribution as we have assumed in this work. Thus, we can treat $A_{\rm phy}$ as an area of a *double-sided* planar probe, and equation (7) becomes an EVDF defined from $-\infty$ to ∞ in v_z -space.

We, now, re-estimate n_0 and $T_{\rm eff}$ as the 0th and the 2nd moment of $f_{\rm ez}(v_z)$, respectively. The effective electron temperature $T_{\rm eff}$ is so defined, i.e.

$$T_{\text{eff}} = \frac{m_{\text{e}}}{n_0} \int_{-\infty}^{\infty} dv_z v_z^2 f_{\text{ez}}, \tag{8}$$

to be consistent with the kinetic Bohm criterion derived by Baalrud [4] which is $U_{\rm i} \geqslant \left[(m_{\rm e}/m_{\rm i}) \, n_0^{-1} \! \int_{-\infty}^{\infty} \! {\rm d} v_z v_z^2 f_{\rm ez} \right]^{1/2}$, where $U_{\rm i}$ is the ion fluid speed at the sheath edge.

To aid numerical integrations of $f_{ez}(v_z)$, we interpolate and extrapolate the EVDF by assuming that it is locally Maxwellian in velocity space. This can be easily performed in a plot of $\ln(f_{ez})$ vs v_z^2 , where two neighbouring points, i.e. local in velocity space, can be linearly fit, which is shown as the red line in figure 3.

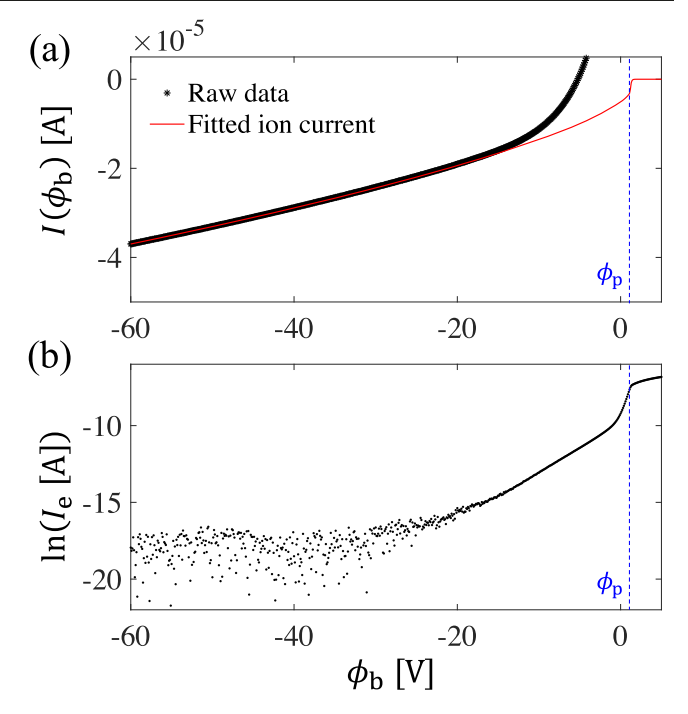


Figure 4. An example of (a) the raw I-V characteristic from figure 2 (black asterisks) and the estimated ion current I_i (red solid), and (b) semi-log plot of the electron current I_e obtained by subtracting the estimated ion current I_i from the raw I-V characteristic. Notice the scattered (rather than ordered) data points in (b) for $\phi_b < -30 \text{ V}$ where we would expect to have zero electron currents.

With new values of n_0 and $T_{\rm eff}$, we, again, estimate $I_{\rm i}(\eta)$ using equations (2) and (3) with the power law coefficient $a(\rho)$ and exponent $b(\rho)$ being free parameters. The described steps to update n_0 and $T_{\rm eff}$ are continued until a difference compared to the values from the previous iteration becomes less than 0.1%. An example of resulting ion and electron currents is shown in figures 4(a) and (b), respectively, where we obtain $n_0 = 1.53 \times 10^8$ cm⁻³ and $T_{\rm eff} = 0.71$ eV for this case. We see that our power law fitting method for the ion current $I_{\rm i}$ (red line) to the raw I-V characteristic (black asterisks) in the region of large negative bias voltage is excellent. This is also attested by the fact that the electron current $I_{\rm e}$ obtained by subtracting $I_{\rm i}$ from the raw I-V characteristic reaches to a clear noise level, i.e. scattered (rather than ordered) data points, for $\phi_{\rm b} < -30$ V where we would expect to have zero electron currents

Typically, we have two-temperature electrons in our experiments⁷. This can be seen from the example in figure 4(b), where cold and hot electron temperatures are 0.50 and 3.11 eV, respectively, with hot electron density fraction of 0.07. We note that the effective electron temperature as a density weighted harmonic mean of two electron species [37], which is 0.53 eV for this example, is noticeably smaller than that calculated using equation (8), i.e. 0.71 eV. This is because a value

⁷ This may seem to contradict one of the assumptions we have made, which is the local Maxwellian assumption. We emphasize that our Maxwellian assumption is *local* in velocity space which is still valid for bi-Maxwellian distributions.

of the harmonic mean weakly depends on a hot temperature if the difference between cold and hot temperatures are appreciable. Finally, we note that this is a rather extreme example within our database showing large difference, i.e. $0.71 \text{ eV} \text{ vs } 0.53 \text{ eV}.^8$

4.2. Comparisons of our method with others

For the sake of demonstrating goodness of our method for extracting the ion current, we compare it with other existing methods. They are a simple linear fitting method, i.e. $I_{\rm i} = I_{\rm i}^{\rm sat} + c(\phi_{\rm b} - \phi_{\rm p})$ with two free parameters $I_{\rm i}^{\rm sat}$ and the slope c, and using Sheridan's empirical formulae, i.e. equation (5), with one free parameter $I_{\rm i}^{\rm sat}$. Note that unlike ours, these two methods have $I_{\rm i}^{\rm sat}$ as a free parameter whose resultant density may differ from the density estimated using $I_{\rm sat}^{\rm sat}$.

As shown in figure 5(a), all the fitting methods obtain the ion current seemingly well following close to the raw I-V characteristic (black asterisks) for sufficiently small $\phi_{\rm b}$, of which our method (red) and using the Sheridan's model (green), i.e. equation (5), exhibit the good fit compared to the linear fit that largely overestimates $I_{\rm i}^{\rm sat}$. The selected example has the normalized probe radius $\rho \approx 30$, and fits in the figure are performed in the range of $30 \le \eta \le 50$. These conditions are within the simulation domain of the Sheridan's work [21].

A semi-log plot of the corresponding electron currents I_e is shown in figure 5(b). As mentioned above and similar to figure 4, our method successfully estimates I_e (red) where clear noise levels are observed for $\phi_b < -30$ V. As I_e is estimated by subtracting the fitted I_i from the raw I-V characteristic, negative values of I_e inevitably exist. To avoid negative values inside a log function, we have plotted $\ln |I_e|$ here. The effects of taking absolute values of I_e from the linearly fitted ion current (blue) are clearly manifested by the fact that I_e decreases towards zero near $\phi_b \approx -35$ V and ≈ -50 V, where the negative I_e for the region in between the two points is visualized. Similar effect is also observed for using Sheridan's empirical formulae (green), while such effect is less pronounced for our method.

The plasma parameters estimated by the different fitting methods are summarized in table 1. As observed in figure 5(a), the fitted $I_i^{\rm sat}$ from the linear fit (blue) and using Sheridan's empirical formulae (green) overestimates that from the power law fit (red) which guarantees equal electron and ion densities. Therefore, those two methods overestimate n_i compared to n_e (the 0th moment of $f_{ez}(v_z)$) contradicting the assumption on the quasi-neutrality of plasmas [2, 38]. Since our plasmas exhibit the two-temperature electrons, we have specified the hot electron temperature $T_{\rm eh}$ and the fraction of the hot electron to the total electron density $n_{\rm eh}/n_e$. Compared with our power law method, the other two methods overestimate

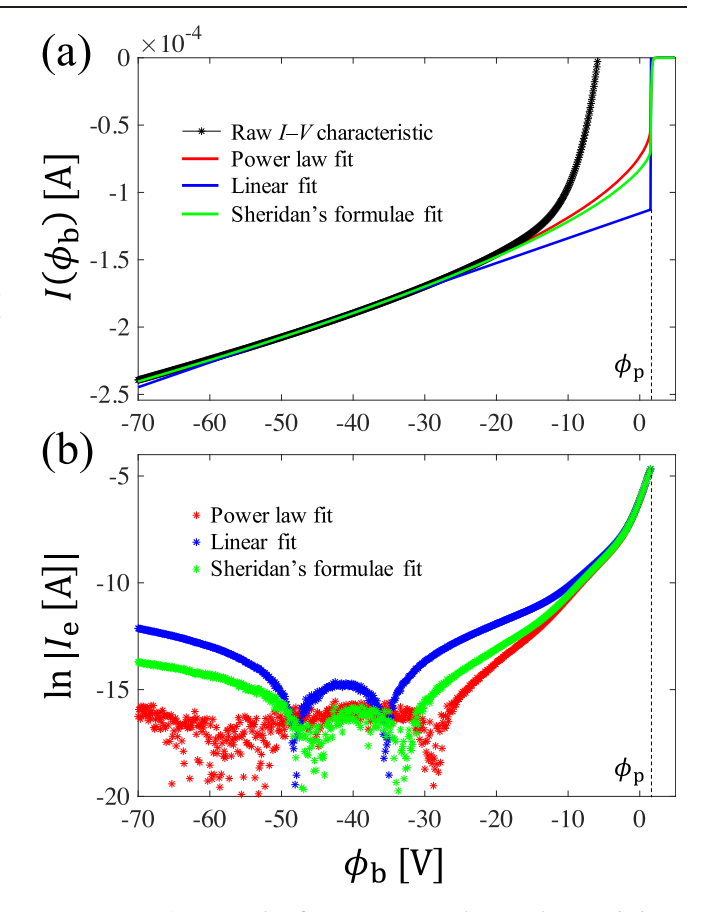


Figure 5. (a) An example of a raw (measured) I-V characteristic (black asterisks) and estimated ion current I_i using the power law fit (red), linear fit (blue), and the Sheridan's empirical formulae fit [21], i.e. using equation (5) (green). The range of the curve fit is $30 \le \eta \le 50$ for all cases. (b) A semi-log plot of the corresponding electron current I_e calculated by subtracting I_i from the raw I-V characteristic with the same colour code as in (a). The normalized probe radius is $\rho \approx 30$ for all cases.

 $T_{\rm eh}$ and underestimate $n_{\rm eh}/n_{\rm e}$, large enough to affect investigating physical phenomena concerned with hot electron species. $T_{\rm eff}$ (the 2nd moment of $f_{\rm ez}(v_z)$) is nearly unaffected by the methods applied, however, if the number density of the hot electrons has large fraction on electron species or $T_{\rm eh}$ is much larger than $T_{\rm ec}$, the discrepancy in $T_{\rm eff}$ between the fitting methods could be conspicuous and affect results concerning the Bohm criterion. The results in the fitting range of $50 \le \eta \le 70$ are also shown, which we found another advantage of our method; it is less sensitive to the selected fitting range than the linear fitting method. This is elaborated further in section 5.

In order to quantitatively compare goodness of the fit, we calculated mean squared error MSE $\equiv \sum_{j=1}^N [I_j^m - I_j^f]^2/N$ for N data points within the selected range, i.e. either $30 \leqslant \eta \leqslant 50$ or $50 \leqslant \eta \leqslant 70$, where I_j^m is the measured probe current, and I_j^f is the fitted ion current. Our power law fitting method exhibits the smallest MSE, which is approximately 10–40 times and 200–1000 times smaller compared to using Sheridan's formulae and the linear fitting method, respectively.

 $^{^8}$ Of course, we are free to choose how to *define* $T_{\rm eff}$ as long as it is associated with the second moment of the distribution function; however, we must carefully define $T_{\rm eff}$ if it is used to make physics interpretations. In this work, different choice of $T_{\rm eff}$ does not change our overall conclusion.

Table 1. Comparison of the estimated plasma parameters and the goodness of the fit as mean squared error (MSE) from three different methods on extracting ion current from the I-V characteristic shown in figure 5(a): (1) power law fit (our proposed method), (2) linear fit (conventionally widely used method), and (3) Sheridan's formulae (based on numerical results). Each method is fitted to two different ranges, i.e. $30 \le \eta \le 50$ and $50 \le \eta \le 70$, to show sensitivity of estimating plasma parameters on the subjectively selected range. Here, $T_{\rm ec}$, $T_{\rm eh}$ and $T_{\rm eff}$ denote the cold, the hot and the effective electron temperature, respectively. $n_{\rm e}$ and $n_{\rm i}$ are the densities of electrons and ions, respectively; while $n_{\rm eh}$ is the density of hot electrons.

Fitting method	Fitting range	T _{ec} (eV)	T _{eh} (eV)	$n_{\rm e}~(10^9~{\rm cm}^{-3})$	$n_{\rm eh}/n_{\rm e}$	$n_{\rm i}~(10^9~{\rm cm}^{-3})$	$T_{\rm eff}~({\rm eV})$	MSE (10^{-6} mA^2)
Power law fit	$30 \leqslant \eta \leqslant 50$	0.81	2.75	2.15	0.089	2.15	1.06	0.007
	$50 \leqslant \eta \leqslant 70$	0.81	2.74	2.15	0.090	2.15	1.06	0.031
Linear fit	$30 \leqslant \eta \leqslant 50$	0.88	3.40	2.15	0.060	4.57	1.07	7.728
	$50 \leqslant \eta \leqslant 70$	0.91	3.93	2.15	0.047	5.19	1.08	5.660
Sheridan's formulae fit	$30 \leqslant \eta \leqslant 50$	0.83	2.88	2.15	0.081	2.81	1.07	0.307
	$50 \leqslant \eta \leqslant 70$	0.83	2.86	2.15	0.082	2.80	1.07	0.228

5. Results: power law dependence of $\alpha_{\rm EE}$

We have conducted experiments with the discharge current varying from 0.002 to 2.2 A to alter the normalized probe radius ρ , as mentioned in section 3. For our experimental conditions, the normalized probe radius varied between $4.14 \leqslant \rho \leqslant 60.88$, within which we verified a power law dependence of the normalized edge effect area $\alpha_{\rm EE}$.

5.1. Verifying a power law dependence of $\alpha_{\rm EE}$ on η

A simple way to verify a power law dependence of $\alpha_{\rm EE} = (I_{\rm i} - I_{\rm i}^{\rm sat})/I_{\rm i}^{\rm sat} = a\eta^b$ from equations (2) and (3) on the normalized bias η is to plot $\alpha_{\rm EE}$ vs η in log-log scale and examine linearity. Direct examination of $\alpha_{\rm EE}$ obtained by our method described in section 4.1 will not be fair verification as it has been constrained (or assumed) to follow a power law. We therefore defined a normalized experimental current $\alpha_{\rm EE}^{\rm ex}$, related of course to the effective current collecting area, using the total probe current $I_{\rm tot}$ (= $I_{\rm e}$ - $I_{\rm i}$) as

$$\alpha_{\rm EE}^{\rm ex} = \frac{-I_{\rm tot} - I_{\rm i}^{\rm sat}}{I_{\rm i}^{\rm sat}}$$

$$\approx \frac{I_{\rm i} - I_{\rm i}^{\rm sat}}{I_{\rm i}^{\rm sat}} = \alpha_{\rm EE} \quad \text{for } \eta \gg 1. \tag{9}$$

We estimated $I_{\rm i}^{\rm sat}$ without invoking an assumption of a power law dependence; thus, we defined a new variable $\alpha_{\rm EE}^{\rm ex*}$ as

$$\alpha_{\rm EE}^{\rm ex*} = \alpha_{\rm EE}^{\rm ex}|_{I_{\rm i}^{\rm sat} = \kappa\sqrt{2\pi}\sqrt{\frac{m_{\rm e}}{m_{\rm i}}}I_{\rm tot}(\phi_{\rm b} = \phi_{\rm p})},$$
 (10)

where the ion saturation current was approximated based on the total current of the I-V characteristic, which is a reasonable approach as $I_{\rm tot}(\phi_{\rm b}=\phi_{\rm p})\approx I_{\rm e}^{\rm sat}$. As $\alpha_{\rm EE}^{\rm ext}$ can be obtained solely based on the experimentally measured quantities without invoking any assumptions, we examined it to provisionally identify behaviour of the effective current collecting area. Figure 6(a) shows how $\alpha_{\rm EE}^{\rm ext}$ depends on η^* , where η^* is the normalized bias voltage by the initial $T_{\rm eff}$ (see section 4.1), for plasmas with various discharge currents. Even if $\alpha_{\rm EE}^{\rm ext}$ is a crude proxy of $\alpha_{\rm EE}$, we identify good linearity for $\eta^* \gtrsim 25$, which justifies our method for estimating the ion current, i.e. the power law fitting method, described in section 4.1.

Given the observed power law dependence of $\alpha_{\rm EE}^{\rm ex*}$, we employed the iterative procedure of our method and obtained electron and ion currents separately to acquire consistent values of n_0 and $T_{\rm eff}$. This allowed us to calculate $I_{\rm i}^{\rm sat}$ using equation (1) and $\alpha_{\rm EE}^{\rm ex}$ in equation (9). A plot of $\alpha_{\rm EE}^{\rm ex}(\eta)$ in log-log scale is shown in figure 6(b) for values of the normalized probe radius ρ from 4.14 (blue) to 60.88 (red). The linearity was, again, clearly observed for $\eta \gtrsim 25$, i.e. unshaded area in figure 6(b). It is now evident why we have obtained similar results for the power law fit with two different ranges in table 1: one prominent linear line persists over a wide range of η as long as $\eta \gtrsim 25$ as shown in figure 6, thereby removing subjectivity of selecting a fitting range.

For small η in the shaded area in figure 6(b), electrons are not fully repelled by the probe bias, which we can designate as the intermediate region of the I-V characteristic, resulting in the deviation from the verified power law relation. As ρ increased, a larger value of η was required to reach a valid range of the power law fit as indicated by yellow \star signs in figure 6(b). Hence the power law model for the ion current cannot be validated for this intermediate region where the nonnegligible electron currents hinder the exclusive acquisition of the ion current. Nevertheless, we extrapolated the verified power law curve with given boundary condition I_i^{sat} to estimate I_i over the whole region ($\eta \geqslant 0$) to employ our iterative analyses.

5.2. Parameterizing $\alpha_{\sf EE}$

As have been discussed in previous sections, for large negative biases ($\eta \gg 1$) a double planar probe collects the ion current I_i with an expanded ion collecting area following a power law as in equations (2) and (3). Therefore, by performing a linear fit to log $\alpha_{\rm EE}^{\rm ex}$ as a function of log η in the range of $\eta \gtrsim 25$, we obtained the ordinate-intercept and the slope as the power law coefficient a and exponent b, respectively.

Figure 7(a) shows the fitted power law coefficient a (triangles) as a function of the normalized probe radius ρ together with the calculated a using equations (4) and (5) (dotted and dashed lines, respectively), which, while showing qualitatively similar behaviour, also demonstrate discrepancies. Comparing the results in the limit of small ρ , we find that a increases without limit as ρ approaches to zero, which is consistent with the Sheridan's simulation result. This is limit in which the

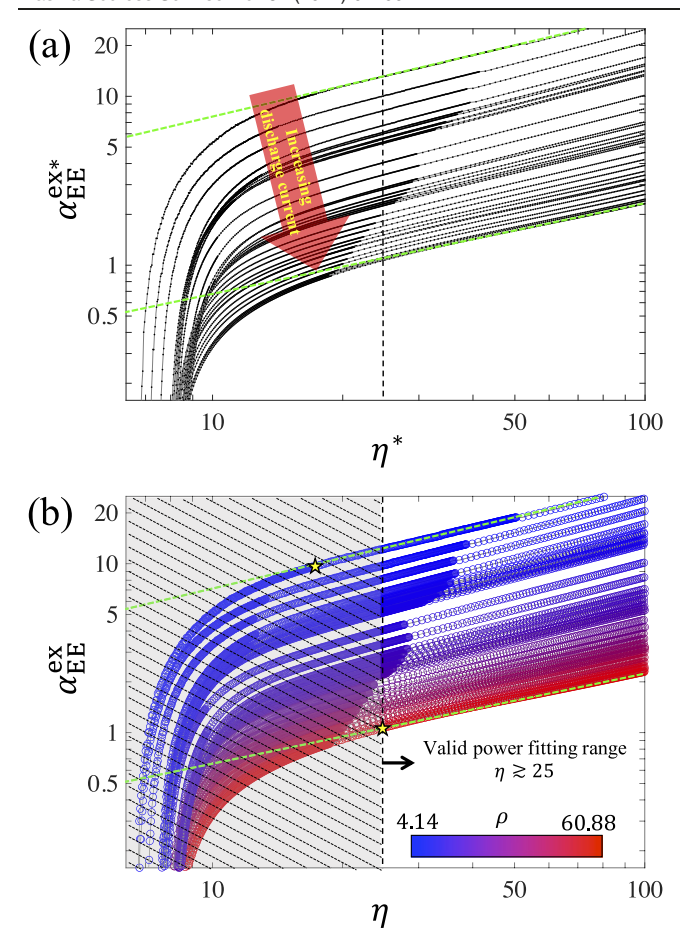


Figure 6. Log-log scale plots of normalized currents defined to examine the behaviour of $\alpha_{\rm EE}$. (a) Estimated $\alpha_{\rm EX}^{\rm ex*}$ as a function of normalized bias voltage η^* for discharge currents varying from 0.002 to 2.2 A, demonstrating good linearity for $\eta^* \gtrsim 25$ (the vertical dashed line is drawn at this value); (b) same as (a) except that $\alpha_{\rm EE}^{\rm ex}$ and η estimated by our iterative method described in section 4.1 are used where different colours represent different values of the normalized probe radius ρ varied by changing the discharge current. Good linearity is also confirmed for $\eta \gtrsim 25$. Shaded area indicates a region where electron contribution is non-negligible resulting in failure of linearity, which is also indicated by yellow \star signs for $\rho=4.14$ and 60.88 as examples. Green dashed lines in both (a) and (b) are examples of fitted linear lines. Refer to the text for more detailed descriptions of $\alpha_{\rm EE}^{\rm ex}$ and $\alpha_{\rm EE}^{\rm ex}$ as well as η^* and η .

sheath effectively becomes spherical [21]. This is also supported by Karamcheti's work [22] showing that a spherical probe is also expected to have this diverging characteristic of a. As ρ increases, both the empirically estimated value of a and model values diminish; however, it is clear that Sheridan's model does not agree with the empirical results: the model underestimates the experimental value, and the discrepancy exceeds the uncertainty.

The power law exponent b is shown in figure 7(b) as a function of ρ . Sheridan's results are also shown with the dotted and dashed lines. Two comparisons are important to observe. First, both the empirically estimated exponent b and the model value are less than 1, that is, the normalized edge effect area grows less than linearly, which is the conventional estimate used to subtract ion current from probe current. Second, while,

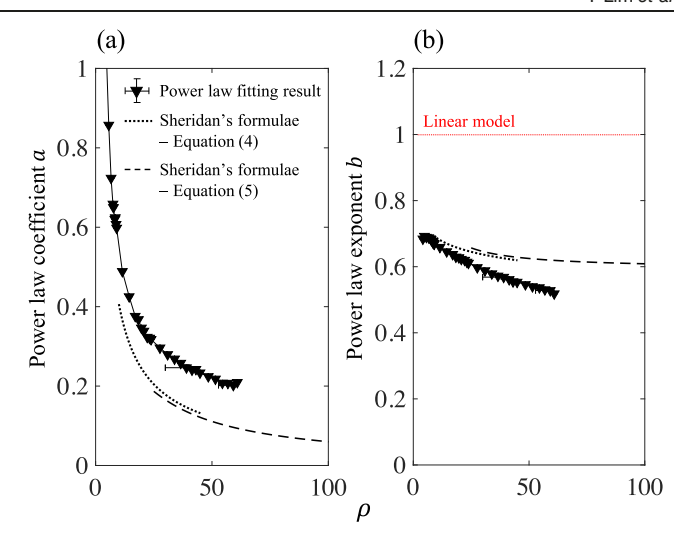


Figure 7. Dependence of the power law (a) coefficient a and (b) exponent b as a function of ρ from experiments (triangles) and Sheridan's simulation results using equation (4) for $10 \le \rho \le 45$ (dotted line) and equation (5) for $25 \le \rho \le 200$ (dashed line). The red dotted horizontal line in (b) represents the linear ion current model. The sizes of the errorbar for the power law fit results are within the size of the symbol.

again, in the limit of small ρ , the empirical and model values agree, the two disagree, with the discrepancy exceeding the uncertainty, $\rho \gg 1$. Further, the model value overestimates the experimentally obtained exponent. This is possibly due to idealized conditions in the simulations, where Boltzmann electrons and collisionless cold ions are assumed [21].

Johnson and Holmes have shown experimentally for a onesided planar probe that $b \approx 0.75$ for plasma densities varying from $0.7\text{--}4 \times 10^{11}~\text{cm}^{-3}$ with a theoretical justification using the Child-Langmuir law [6]. The normalized probe radius ρ is estimated to be \sim 100 in their work which means that their values of b are much larger than what we have observed; while the power law coefficient a is estimated to be of the order of $\mathcal{O}(10^{-2})$ which is far smaller than our values⁹. One may argue that the difference can be attributed to a type of the planar probe, i.e. double-sided vs one-sided; however, we think that there are other possible reasons associated with experimental conditions such as material of the probe, cleanness of the probe, types of working gas, collisionality of plasmas due to different neutral pressures and so on. In fact, we show that the power law exponent b indeed changes with different pressures in section 6. This is another good reason why one should let the power law parameters (a and b) be fitting parameters as described in section 4.1, rather than relying uncritically on equations (4) and (5).

As Sheridan has found an asymptotic behaviour of $\alpha_{\rm EE}$ scaling as $\sim \rho^{-1}$ for constant values of the normalized bias voltage η [21], we have also examined the relation as shown in figure 8 from $\eta=10$ to 100. Our data shows a good linear relation in log-log scale with a scaling factor of ~ -0.9 for wide ranges

⁹ Johnson and Holmes do not explicitly provide values of ρ nor a in their work. We have estimated them based on information provided in reference [6] with an assumption that electron temperature did not vary much.

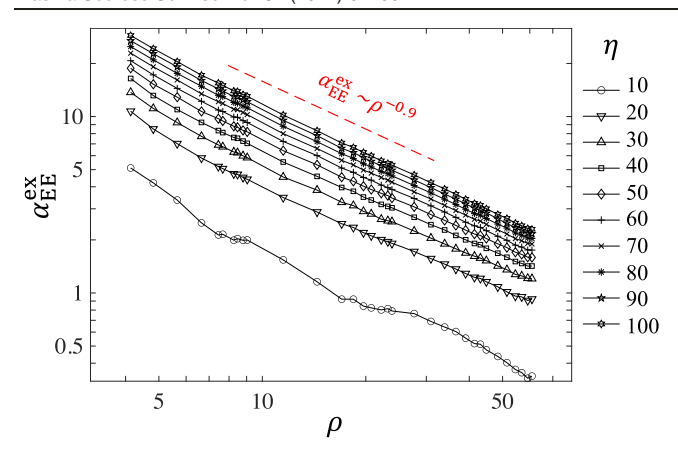


Figure 8. Relation between $\alpha_{\rm EE}^{\rm ex}$ and ρ for constant values of η from 10 to 100, demonstrating $\alpha_{\rm EE}^{\rm ex} \sim \rho^{-0.9}$ for investigated experimental conditions. Refer to text for explanation of different behaviour for $\eta=10$ case.

of η and ρ , in qualitative agreement with the model except, of course, for low values of η (see for example the $\eta=10$ case). As noted in section 5.1, this is owing to electron contributions as the bias voltage is not large enough to repel all the incoming electrons. Although exact values of the scaling factor is slightly different between our experimental data and the simulations [21], we find that the asymptotic behaviour, i.e. $\alpha_{\rm EE} \to 0$ as $\rho \to \infty$, is consistent with our intuition that the larger the probe radius, the more negligible the increase in effective current collection area becomes.

6. Discussion: effects of neutral pressure on $\alpha_{\rm EE}$

We have examined dependence of $\alpha_{\rm EE}^{\rm ex}$ on the neutral pressure as well. Figure 9 shows our experimental observation for Ar pressures of 0.04 Pa (\approx 0.3 mTorr) (black), 0.13 Pa (\approx 1.0 mTorr) (red) and 1.20 Pa (\approx 9.0 mTorr) (blue). Within investigated experimental conditions it is evident that higher neutral pressures always yields smaller $\alpha_{\rm EE}^{\rm ex}$ at a given ρ and η , which is qualitatively consistent with the simulation result by Voloshin *et al* [30] where ion elastic and charge exchange collisions with the Ar neutral particles were included. For the plasmas we generated, typically, the absolute extent of the sheath shrinks as the neutral pressure rises because of the decreasing electron temperature and the rising plasma density. However, we preclude such effects in our discussions since figure 9 is shown in the normalized ρ - η space.

As an attempt at understanding the effects of pressure further, in figure 10(a) we plot η vs ρ on log-log scales for fixed $\alpha_{\rm EE}^{\rm ex}$, and we show a family of such curves for different values of log $\alpha_{\rm EE}^{\rm ex}$. The pressure was fixed at 0.13 Pa. In the valid region of the power law ($\eta \gtrsim 25$), we notice at least three features: (1) all the lines are linear, (2) the slopes are very similar for different values of log $\alpha_{\rm EE}^{\rm ex}$, and (3) the lines are presented in equidistant steps of log $\alpha_{\rm EE}^{\rm ex}$ with a common difference of ~ 0.15 . This means that we can approximate log η as

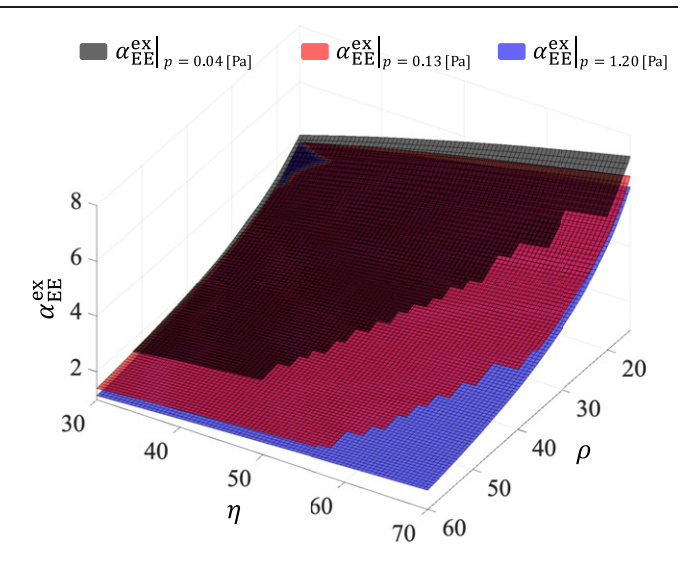


Figure 9. Contour plot of $\alpha_{\rm EE}^{\rm ex}$ as a function of η and ρ for Ar pressures of 0.04 Pa (black), 0.13 Pa (red) and 1.20 Pa (blue). As Ar pressure increases, $\alpha_{\rm EE}^{\rm ex}$ decreases.

$$\log \eta \approx S \log \rho + B(\log \alpha_{\rm EE}^{\rm ex} - \log C), \tag{11}$$

where S denotes a common slope of the linear lines, and C is a constant. The coefficient B controls the relative distance between the lines, and it must be that $B \approx 1/b$ to be consistent with experimentally verified (in section 5.1) power law $\alpha_{\rm EE}^{\rm ex} = a\eta^b$. Notice from figure 7(b) that b is a weak function of ρ and slightly increases as ρ decreases. This is also noticeable in figure 10(a), i.e. gaps between the lines become marginally narrower for smaller ρ .

By rearranging equation (11) for α_{EE}^{ex} , we get

$$\alpha_{\rm EE}^{\rm ex} \approx C \rho^{-bS} \eta^b.$$
 (12)

To introduce pressure dependence of $\alpha_{\rm EE}^{\rm ex}$ as shown in figure 9, we conjecture that the slope S and constant C are functions of the pressure. Comparing equation (12) with equation (3), we have

$$a(\rho, p) \approx C(p)\rho^{-b(\rho)S(p)}$$
. (13)

From figure 8 we have inferred based on the measured data that $\alpha_{\rm EE}^{\rm ex} \sim \rho^{-0.9}$ which suggests that $a \sim \rho^{-0.9}$ since η is kept constant and the power law exponent b is a weak function of ρ . This is consistent with equation (13) for $b \approx 0.6$ and $S \approx 1.5$ resulting in $\rho^{-bS} \approx \rho^{-0.9}$ for the pressure of 0.13 Pa. Figure 10(b) further corroborates our conjecture. It shows that increasing pressure from 0.04 Pa (black) to 0.13 Pa (red) to 1.20 Pa (blue) shifts the lines up, i.e. changes C, for $\alpha_{\rm EE}^{\rm ex} = 2.5$ (circle), 3.5 (triangle) and 5.0 (square). We observe though that the slope seem to change significantly only for the highest pressure case, 1.20 Pa.

For the pressures we investigated, the mean free path of ion–neutral collision $\lambda_{\rm mfp}$ (including both elastic and charge-exchange collisions) were approximately 100 mm, 30 mm and 3 mm for Ar pressure of 0.04 Pa, 0.13 Pa and 1.20 Pa, respectively. The sheath thickness was typically less than 10 mm, similar to other works [39–42] in similar plasma conditions

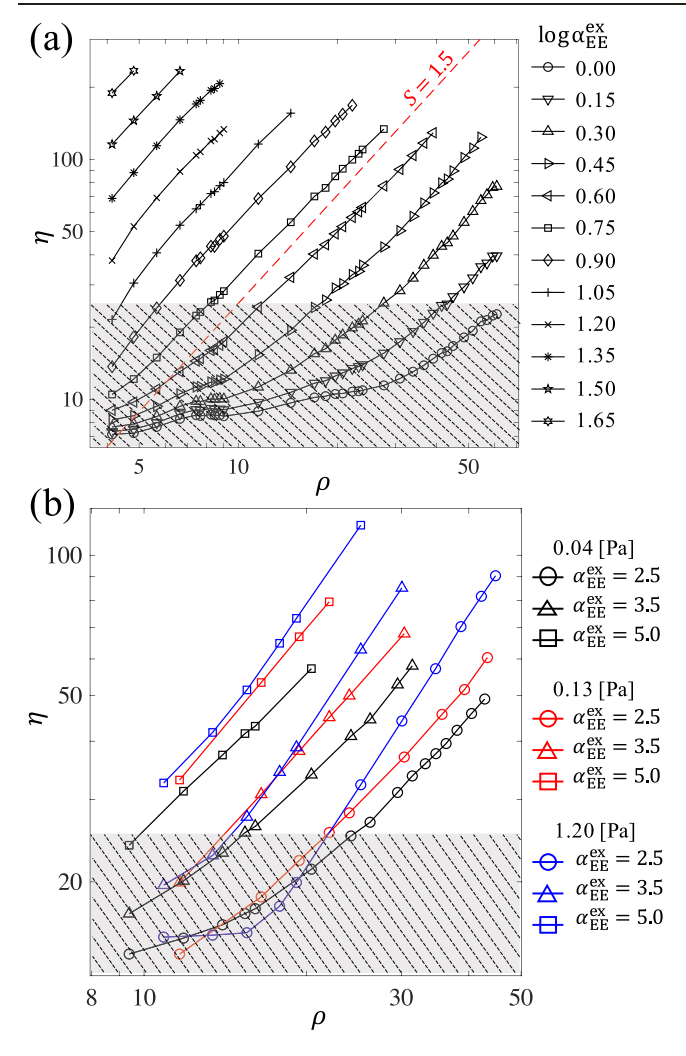


Figure 10. The normalized bias η vs the normalized probe radius ρ in log-log scale (a) for Ar pressure of 0.13 Pa with various constant values of log $\alpha_{\rm EE}^{\rm ex}$ showing a constant slope $S\approx 1.5$ and (b) for Ar pressures of 0.04 Pa (black), 0.13 Pa (red) and 1.20 Pa (blue) with three constant values of log $\alpha_{\rm EE}^{\rm ex}$. Shaded areas indicate invalid regions of the power law, i.e. $\eta\gtrsim 25$.

described in this work. Thus, we expect non-negligible collisions within the sheath only for 1.20 Pa case, and we expect there to be a change in the slope *S* for that case.

In this work, we have used $\kappa=0.6$ regardless of different pressures. As mentioned earlier in the footnote, variation in κ could be bundled into the constants parameterizing $\alpha_{\rm EE}^{\rm ex}$. Different pressures discharges may have slightly different presheath potential structures that could lead to variations in κ [3, 29, 43] in equation (1). While this could effectively change the constant C as in figure 10(b), we did not examine this effect. Correct value of κ may be smaller for more collisional presheath as the required voltage drop from the bulk plasma to the sheath edge for ions to obtain the Bohm speed can be larger than collisionless case [3, 44, 45]. We leave detailed investigation on change of κ associated with a neutral pressure as a future work.

7. Summary and conclusion

We have experimentally investigated the effective ion collecting area of a double-sided planar Langmuir probe for which the normalized edge effect area is shown to have a power law dependence on the probe bias voltage. This is the first experiment that benchmarks details of Sheridan's model, and its prediction of the power law dependence of the sheath expansion for the ion branch of a planar Langmuir probe. For the practical applicability of the power law dependence, the iterative method of analyzing an I-V characteristic is presented where the ion current is estimated by fitting the power law to the normalized edge effect area. Our method on estimating the ion current implicitly constrains the quasi-neutrality of plasmas unlike other methods we have compared with, i.e. a linear fitting method and using Sheridan's empirical formulae. From the comparison, we have confirmed that our method exhibits the best fit results with negligible sensitivity to the fitting ranges while the linear fitting method is subjective to a selected fitting range.

To preclude assumptions as much as possible for verifying the power law dependence, we have examined behaviour of the edge effect area solely based on measured quantities, and then applied our iterative method to infer fully consistent plasma parameters. Our thorough investigations indicate that the normalized edge effect area has the power law dependence for the normalized probe bias $\eta \gtrsim 25$ within the experimental conditions of the normalized probe radius $4.14 \le \rho \le 60.88$.

Behaviour of the power law coefficient a and exponent b parameterized by the best fit to $\alpha_{\rm EE}^{\rm ex}$ as a function of the normalized probe radius ρ is investigated. A spherical sheath is expected when ρ approaches to zero, and the observed diverging characteristic of a with decreasing ρ is consistent with the expectation. As ρ increases, sheath expansion should become less important which corresponds to the observed asymptotic behaviour of a. The exponent b is found to have weak and negative dependency on ρ , and its value is less than one, which indicates the conventional method of linearly extrapolating to the plasma potential to find an estimate of an ion saturation current is in error. Qualitative behaviour of both a and b are similar to the Sheridan's empirical formulae while the values are slightly different. This implies that results obtained with limited physics, e.g. simulation, may not be generally applicable to experiments (although they can be good guides), and fitting parameters should be found experimentally.

We have also investigated effects of the neutral gas pressure, i.e. ion–neutral collisions, to the normalized edge effect area with three different pressures of 0.04 Pa (≈ 0.3 mTorr), 0.13 Pa (≈ 1.0 mTorr) and 1.20 Pa (≈ 9.0 mTorr). Based on the observed features, we have conjectured different mechanisms for modifying the normalized edge effect area whether we have collisional presheath or collisional sheath. Our experimental data suggests that a collisional presheath changes a required voltage drop from the bulk to the sheath edge for ions to have the Bohm velocity; while a collisional sheath tends to force the normalized edge effect area to be more

sensitive to the Debye length. These are consistent with our simple intuition.

As a final remark, we emphasize that our method to fit the ion current is an entirely new approach valid for plasmas with equal densities of positive ions and electrons. The method does not rely on any of numerical results and obtains plasma density and an electron temperature solely based on experimentally obtained data. Furthermore, the iterative approach in our method guarantees consistency with the data, providing correct plasma parameters within experimental uncertainties.

Acknowledgments

This work is supported by National R & D Program through the National Research Foundation of Korea (NRF) funded by the Ministry of Science and ICT (Grant Nos. NRF-2020M1A7A1A03016161 and NRF-2021R1A2C2005654). GS is supported by US National Science Foundation (NSF PHY-1804240 and NSF PHY-2108636). CSY is supported by National Natural Science Foundation of China (Contract No. 11875285).

Data availability statement

The data generated and/or analysed during the current study are not publicly available for legal/ethical reasons but are available from the corresponding author on reasonable request.

ORCID iDs

Yegeon Lim https://orcid.org/0000-0003-1143-7227 Greg Severn https://orcid.org/0000-0002-4794-5170 Chi-Shung Yip https://orcid.org/0000-0003-4475-8000 Y-c Ghim https://orcid.org/0000-0003-4123-9416

References

- [1] Mott-Smith H M and Langmuir I 1926 Phys. Rev. 28 727
- [2] Godyak V A and Alexandrovich B M 2015 J. Appl. Phys. 118 233302
- [3] Riemann K U 1991 J. Phys. D: Appl. Phys. 24 493
- [4] Baalrud S D and Hegna C C 2011 Plasma Sources Sci. Technol. 20 025013
- [5] Sheridan T E and Goree J A 1989 IEEE Trans. Plasma Sci. 17 884
- [6] Johnson J D and Holmes A J T 1990 Rev. Sci. Instrum. 61 2628
- [7] Gunn J P, Boucher C, Stansfield B L and Savoie S 1995 Rev. Sci. Instrum. 66 154

- [8] Tsui C K, Boedo J A and Stangeby P C (TCV Team) 2018 Rev. Sci. Instrum. 89 013505
- [9] Bernstein I B and Rabinowitz I N 1959 Phys. Fluids 2 112
- [10] Lam S H 1965 Phys. Fluids 8 73
- [11] Chen F F 1965 J. Nucl. Energy C 7 47
- [12] Laframboise J G 1966 Theory of spherical and cylindrical Langmuir probes in a collisionless, Maxwellian plasma at rest *Technical Report 100* (Toronto: University of Toronto Institute for Aerospace Studies)
- [13] Parrot M J M 1982 Phys. Fluids 25 2388
- [14] Rogers J H, De Groot J S and Hwang D Q 1992 Rev. Sci. Instrum. 63 31
- [15] Stamate E and Sugai H 2005 Phys. Rev. E 72 036407
- [16] Sheridan T E 2008 J. Phys. D: Appl. Phys. 42 015212
- [17] Stamate E and Yamaguchi M 2015 Appl. Phys. Lett. 107 094106
- [18] Hershkowitz N 1989 How Langmuir probes work *Plasma Diagnostics* vol 1 ed O Auciello and D L Flamm (*Plasma–Materials Interactions*) (New York: Academic)
- [19] Malik S M, Fetherston R P, Sridharan K and Conrad J R 1993 Plasma Sources Sci. Technol. 2 81
- [20] Sheridan T E 2000 Phys. Plasmas 7 3084
- [21] Sheridan T E 2010 J. Phys. D: Appl. Phys. 43 105204
- [22] Karamcheti A and Steinbrüchel Ch 1999 J. Vac. Sci. Technol. A 17 3051
- [23] Narasimhan G and Steinbrüchel Ch 2001 J. Vac. Sci. Technol. A 19 376
- [24] Steinbrüchel Ch 1990 J. Vac. Sci. Technol. A 8 1663
- [25] Mausbach M 1997 J. Vac. Sci. Technol. A 15 2923
- [26] Lee D and Hershkowitz N 2007 Phys. Plasmas 14 033507
- [27] Ghim Y-c and Hershkowitz N 2009 *Rev. Sci. Instrum.* **80** 033502
- [28] Yu P, Cao J, Zhang Z, Liu Y and Lei J 2019 AIAA J. 57 904
- [29] Zhang K, Wang W and Cai G 2021 J. Phys. D: Appl. Phys. 54 245202
- [30] Voloshin D, Rakhimova T and Mankelevich Y 2016 Plasma Sources Sci. Technol. 25 015018
- [31] Chen F F 1965 Plasma Diagnostic Techniques (New York: Academic)
- [32] Chen F F 2016 Introduction to Plasma Physics and Controlled Fusion 3rd edn (New York: Springer)
- [33] Godyak V A, Piejak R B and Alexandrovich B M 1993 J. Appl. Phys. 73 3657
- [34] Koo B-W, Hershkowitz N and Sarfaty M 1999 J. Appl. Phys. 86 1213
- [35] Lim Y et al 2020 Plasma Sources Sci. Technol. 29 115012
- [36] Sheridan T E, Goeckner M J and Goree J 1995 Japan. J. Appl. Phys. 34 4977
- [37] Song S B, Chang C S and Choi D-I 1997 Phys. Rev. E 55 1213
- [38] Merlino R L 2007 Am. J. Phys. **75** 1078
- [39] Lee D, Severn G D, Oksuz L and Hershkowitz N 2006 J. Phys. D: Appl. Phys. 39 5230
- [40] Severn G D, Wang X, Ko E and Hershkowitz N 2003 Phys. Rev. Lett. 90 145001
- [41] Ghim Y-c and Hershkowitz N 2009 Appl. Phys. Lett. 94 151503
- [42] Oksuz L, Lee D and Hershkowitz N 2007 Plasma Sources Sci. Technol. 17 015012
- [43] Meige A, Sutherland O, Smith H B and Boswell R W 2007 Phys. Plasmas 14 032104
- [44] Riemann K U 2003 J. Phys. D: Appl. Phys. 36 2811
- [45] Oksuz L and Hershkowitz N 2005 Plasma Sources Sci. Technol. 14 201